Low-spin lifetime measurements in ^{74}Kr

J. J. Valiente-Dobón,[1,2,*] C. E. Svensson,[2] A. V. Afanasjev,[3] I. Ragnarsson,[4] C. Andreoiu,[2,5] D. E. Appelbe,[6] R. A. E. Austin,[7] G. C. Ball,[8] J. A. Cameron,[7] M. P. Carpenter,[9] R. M. Clark,[10] M. Cromaz,[10] D. Dashdorj,[11] P. Fallon,[10] S. J. Freeman,[9,12] P. E. Garrett,[2,8] A. Görgen,[13] G. F. Grinyer,[2] D. F. Hodgson,[8] B. Hyland,[2] D. Jenkins,[14] F. Johnston-Theasby,[14] P. Joshi,[14] N. S. Kelsall,[14] A. O. Macchiavelli,[10] D. Mengoni,[15] F. Moore,[9] G. Mukherjee,[9] A. A. Phillips,[2] W. Reviol,[16] D. Sarantites,[16] M. A. Schumaker,[2] D. Seweryniak,[9] M. B. Smith,[8] J. C. Waddington,[7] R. Wadsworth,[14] and D. Ward[10]

[1]*INFN Laboratori Nazionale di Legnaro, Legnaro, Italy*
[2]*Department of Physics, University of Guelph, Guelph, Ontario N1G 2W1, Canada*
[3]*Department of Physics and Astronomy, Mississippi State University, Mississippi 39762, USA*
[4]*Lund Institute of Technology, P. O. Box 118 S-221 00 Lund, Sweden*
[5]*Oliver Lodge Laboratory, University of Liverpool, Liverpool L69 3BX, United Kingdom*
[6]*CLRC Daresbury Laboratory, Daresbury, Warrington WA4 4AD, United Kingdom*
[7]*Department of Physics and Astronomy, McMaster University, Hamilton, Ontario L8S 4K1, Canada*
[8]*TRIUMF, 4004 Wesbrook Mall, Vancouver, British Columbia, V6T 2A3, Canada*
[9]*Physics Division, Argonne National Laboratory, Argonne, Illinois 60439, USA*
[10]*Lawrence Berkeley National Laboratory, Berkeley, California 94720, USA*
[11]*North Carolina State University, Raleigh, North Carolina 27695, USA*
[12]*Schuster Laboratory, University of Manchester, Manchester M13 9PL, United Kingdom*
[13]*CEA Saclay, DAPNIA/SPhN, F-91191 Gif-sur-Yvette Cedex, France*
[14]*Department of Physics, University of York, Heslington, York YO10 5DD, United Kingdom*
[15]*Istituto Nazionale di Fisica Nucleare, Sezione di Padova, Padova, Italy*
[16]*Department of Chemistry, Washington University, St. Louis, Missouri 63130, USA*

(Received 13 July 2007; published 27 February 2008)

The nucleus ^{74}Kr has been populated in the ^{40}Ca(^{40}Ca,2$p\alpha$)^{74}Kr fusion-evaporation reaction at a beam energy of 165 MeV and studied using the Gammasphere and Microball multidetector arrays. The lifetimes for low-spin states in the ground-state and two signature-split negative-parity bands were determined using the Doppler-shift attenuation method. These results are discussed together with the lifetimes measured for the high-spin states of these bands and compared with theoretical calculations.

DOI: 10.1103/PhysRevC.77.024312 PACS number(s): 21.10.Re, 23.20.Lv, 27.50.+e, 21.60.Ev

I. INTRODUCTION

Neutron-deficient krypton isotopes are rich in various nuclear structure phenomena. For instance, the ground-state bands of the even-even proton-rich krypton isotopes show deviations from a rotational behavior, due to the presence of shape coexistence, which is supported by the experimental observation of low-lying excited 0^+ states [1–4]. The coexistence of prolate and oblate shapes and their mixing at low angular momentum has been discussed in a number of theoretical approaches [5,6].

In the case of ^{74}Kr, recent Coulomb excitation experiments, which are sensitive to the sign of the quadrupole moments, show that the ground-state band is based on a strongly deformed prolate configuration, whereas the first excited 0^+ state and the rotational structure on top of it have oblate shape [3,4].

In addition, the rotational bands in ^{74}Kr reveal the new phenomenon of nontermination of rotational bands at the maximum spin I_{max}; so far this phenomenon has been observed only in this nucleus [7]. Contrary to the previously known cases of rotational bands, which terminate in a noncollective state when reaching their I_{max} values, the transition quadrupole moments measured using the Doppler-shift attenuation method (DSAM) [8] and the comparison with mean-field calculations strongly suggest that this is not the case in the high-spin rotational bands of ^{74}Kr [7].

In the present work, the interest was focused on lifetime measurements of the low-spin states for the ground-state and the two signature-split negative-parity bands. The lifetimes were determined using the DSAM method.

II. EXPERIMENT

States in ^{74}Kr were populated via the ^{40}Ca(^{40}Ca,2$p\alpha$)^{74}Kr reaction. A 165-MeV ^{40}Ca beam was provided by the ATLAS (Argonne Tandem-Linac Accelerator System) accelerator at Argonne National Laboratory. Thin- and backed-target experiments were performed. The thin target was 350 μg/cm^2 ^{40}Ca sandwiched between two 150-μg/cm^2 Au layers to prevent oxidation during installation of the target in the vacuum chamber. The backed target was a 225-μg/cm^2 ^{40}Ca layer evaporated onto a 13.9-mg/cm^2 Au backing. Gamma rays were detected with 99 Compton-suppressed HPGe detectors of the Gammasphere array [9], in coincidence with charged particles detected and identified with the 95-element CsI(Tl) Microball

*valiente@lnl.infn.it

detector [10]. The hardware trigger required at least four HPGe detectors (after Compton suppression) to fire in prompt coincidence in each experiment. Gamma rays emitted in the decay of excited states of ^{74}Kr were isolated in the offline analysis by selecting events in which two protons and an α particle were detected in prompt coincidence in the Microball detector. Events in which three protons and an α particle (populating ^{73}Br), two protons and two α particles (^{70}Se), or two protons, an α particle, and a neutron (^{73}Kr) were evaporated but one particle escaped detection were removed from this data set by further requiring the sum of the kinetic energies of the two protons and the α particle and the total γ-ray energy detected in the Gammasphere to be consistent with the Q value for the two-proton and one-α evaporation channel [11].

The thin-target data allowed the determination of the lifetimes from the states at the top of the rotational bands, where lifetimes are of the order of tens of femtoseconds. These states decay while the recoil ions are slowing down inside the thin ^{40}Ca target. The centroid-shift Doppler attenuation method was used to measure the lifetimes of the high-spin states in ^{74}Kr. A similar analysis has been perfomed for the ^{76}Kr isotope, where a more detailed description of the experimental method to determined the lifetimes can be found [12]. These results were analyzed and discussed in Ref. [7].

The backed-target data provided additional lifetime information for the lower-spin states. Five matrices were produced at the angles 31.7°, 37.4°, 90.0°, 142.6°, and 148.3°. The program LINESHAPE [14] was used to calculate velocity distributions and fit the line shapes at three angles: one at forward angles, one at 90.0°, and another at backward angles. To increase the statistics at the forward and backward angles, weighted averages of the 31.7°, 37.4° and 142.6°, 148.3° angles, respectively, were used. To simulate the slowing down process the Ziegler and Chu stopping powers [15] were used. The velocity distribution seen by the forward- and backward-angle detectors as a function of time was calculated from 10 000 histories. The program was modified to take into account the initial momenta of ^{74}Kr recoil, resulting from the particle evaporation, and the angular dependence of the detection efficiency of Microball mainly for α particles [16].

III. RESULTS AND DISCUSSION

A partial decay scheme for ^{74}Kr showing the lower-spin states for the ground-state band (GSB) and the favored negative-parity bands, Band A ($\alpha = 1$) and Band B ($\alpha = 0$), is presented in Fig. 1. A more complete level scheme showing the highest-spin states can be found in Ref. [7].

For these lower-spin states, the backed-target data were used to determine the lifetimes. The spectra were obtained by gating on transitions above the level of interest. The side feeding above the gating transitions was modeled using a cascade of four transitions of adjustable lifetimes. Figure 2 shows the fit to the line shape of the 954-keV transition of the favored negative-parity band (Band A). The lifetimes of the lowest-spin states could not be determined because a large fraction of the decays took place when the recoil was completely stopped. Thus, the transitions show a sharp peak,

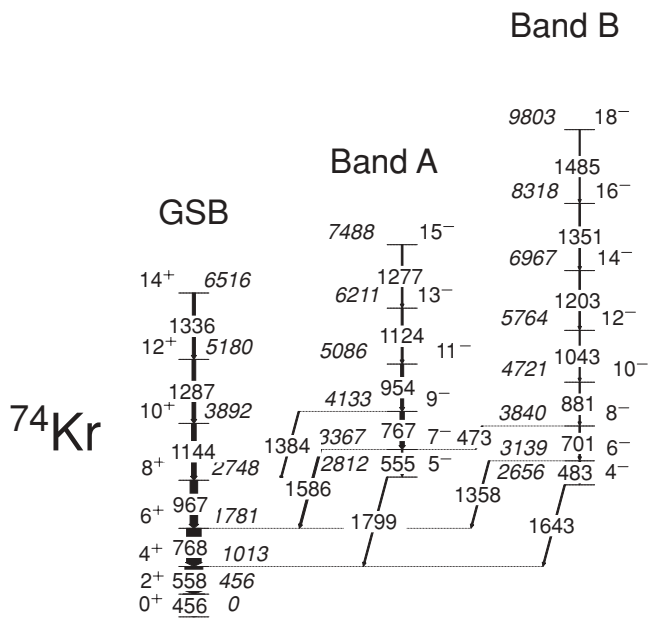

FIG. 1. Partial level scheme, showing only the lower-spin states, for ^{74}Kr. The energies of the γ-ray transitions are given in keV and the arrow widths are proportional to relative γ-ray intensities. A level scheme showing higher-spin states can be found in Ref. [7].

with no shape that could be used to determine the lifetime. The contribution of the contaminants to the line shape was determined using the intensity ratio obtained from the spectra at 90°, where no angular distributions were taken into account. The lifetimes extracted from the line shapes can be used to determine the transition quadrupole moments (Q_t) via the equation

$$\tau^{-1} = 1.2195 Q_t^2 E_\gamma^5 |\langle I K 20 | (I-2) K \rangle|^2, \qquad (1)$$

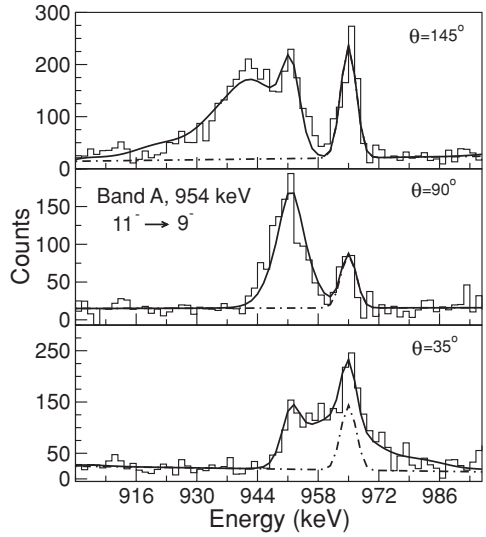

FIG. 2. Line-shape fit in ^{74}Kr for the favored negative-parity band (Band A) transition, 954 keV, from the backed-target data. The top, middle, and bottom panels correspond to line shapes at the mean angles 145°, 90°, and 35°, respectively. The dash-dotted line shows a contaminant peak.

TABLE I. Transition quadrupole moments Q_t for the ground-state band (GSB), Band A, and Band B in ^{74}Kr, deduced from the current data, as a function of spin. These results are compared with those of previous works.

	I^π	E_γ (keV)	τ (ps) (Current)	Q_t (eb) (Current)	Q_t (eb) (Previous)
GSB	6^+	768	0.770 ± 0.040	$3.57^{+0.09}_{-0.08}$	3.08 ± 0.23[a]
	8^+	967	0.280 ± 0.020	$3.25^{+0.11}_{-0.06}$	3.24 ± 0.17[a]
	10^+	1144	0.130 ± 0.020	$3.14^{+0.19}_{-0.18}$	3.18 ± 0.12[a]
Band A	11^-	954	0.190 ± 0.090	$3.99^{+0.09}_{-0.08}$	2.80 ± 0.10 [13]
Band B	10^-	881	0.330 ± 0.020	$3.80^{+0.14}_{-0.12}$	–
	12^-	1043	0.158 ± 0.013	$3.50^{+0.14}_{-0.09}$	–
	14^-	1203	0.095 ± 0.012	$3.14^{+0.25}_{-0.15}$	–

[a]Experimental average value measured in previous RSSD and DSAM experiments [2] (and references therein).

where τ is the lifetime measured in picoseconds, E_γ is the γ-ray transition energy in MeV, Q_t is in (eb), I and K appearing in the Clebsch-Gordan coefficient are the angular momentum of the initial state and the projection of the total angular momentum onto the nuclear symmetry axis, respectively. In the current case the value used for $K = 0$. The DSAM method presents an uncertainty in the lifetime measurements due to the treatment of the stopping powers in the LINESHAPE code. Therefore, the absolute value of transition quadrupole moments, Q_t, is subject to an error of 10–15%. Table I summarizes the Q_t values and lifetimes τ measured with the thick-target data for the GSB, the favored negative-parity bands Band A and Band B. These results are compared with previous works.

The interpretation of the Q_t values for the low-spin states measured in this work (see Table I), will be done together with the known Q_t values for higher-spin states and compared with theoretical calculations. Figure 3 shows the measured transition quadrupole moments, Q_t, for the ground-state band (GSB) and the favored negative-parity bands, Band A ($\alpha = 1$) and Band B ($\alpha = 0$). The solid circles correspond to the measured Q_t values obtained in this work using the DSAM thick-target method, meanwhile the open circles correspond to the high-spin Q_t values measured using the DSAM thin-target method [7]. Only statistical error bars are shown. Results of earlier measurements for low-spin states 2^+, 4^+, and 6^+ are shown by open squares [2]. Results for low-medium spins are shown by solid diamonds, see Ref. [13]. The Q_t values measured in this work are not in agreement with the ones measured by Algora *et al*. [13], who determined the Q_t values of the states of interest by gating on the linking transition between the GSB and Band A (see Table I). The gating transition is placed below the state of interest in Ref. [13], and therefore an uncertainty related to the side feedings to the states of interest is added to the Q_t value determination.

The bands in ^{74}Kr have been studied within different theoretical frameworks. The cranked Nilsson-Strutinsky (CNS) approach [17] and cranked relativistic mean-field (CRMF) theory [18] were applied for the study of high-spin properties and nontermination of these bands in Refs. [7,19]. These calculations without pairing reproduce well the rotational properties of observed bands and the high-spin behavior of

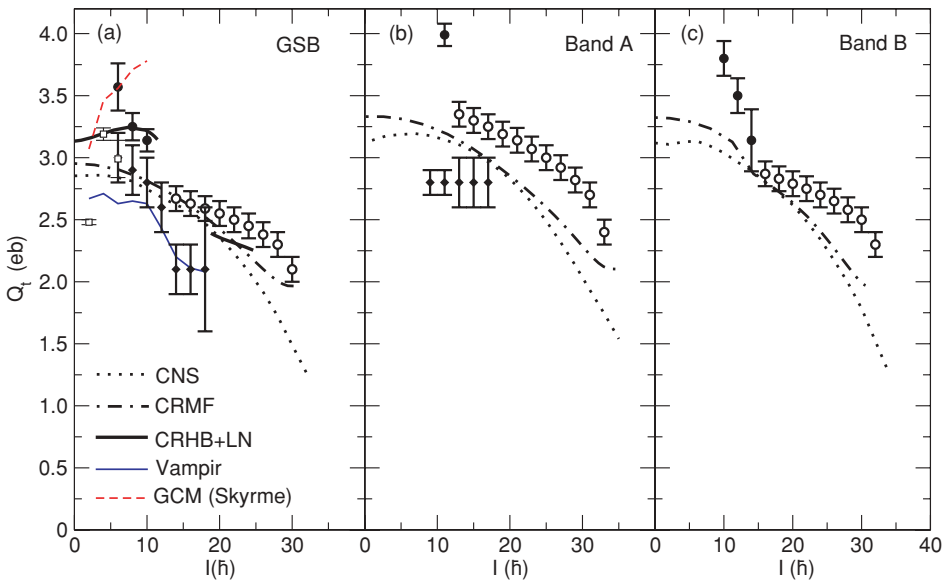

FIG. 3. (Color online) The measured transition quadrupole moments Q_t for (a) the ground-state band (GSB), (b) Band A, and (c) Band B. Solid circles represent the Q_t values obtained from backed-target data in this work, open circles are taken from thin-target data from Ref. [7]. The experimental data from Ref. [2] and Ref. [13] are shown by open squares and solid diamonds, respectively. The results from VAMPIR, CRMF, CNS, CRHB+LN, and GCM (Skyrme) calculations are also shown.

the transition quadrupole moment (see Fig. 3) with CRMF providing a somewhat better description of Q_t than CNS. These calculations associate bands GSB, A, and B with the [2,4] and [3,4] configurations, respectively, where the shorthand notation $[p, n]$ indicates the number of occupied proton (p) and neutron (n) $g_{9/2}$ orbitals. The neglect of pairing at medium and high spin in these bands is well justified because the pairing is negligible above the paired band crossings at $\omega = 0.8$–1.0 MeV/$\hbar$ according to the cranked relativistic Hartree-Bogoliubov (CRHB) calculations of Ref. [19]. For example, the Q_t values for the GSB band obtained in the CRMF and CRHB calculations for spins $I = 18$–$24\hbar$ are almost the same (see Fig. 3). However, these calculations without pairing predict a smooth gradual increase of the Q_t values with decreasing spin, which is in contradiction with experimental data showing a drastic increase of Q_t with decreasing spin below the paired band crossing. We note that the apparent discontinuity between the "high-spin" Q_t values (open circles in Fig. 3) and the "intermediate-spin" values (solid circles) obtained from the line-shape analysis reported here could be partially smoothed by adopting a model with a more rapid decrease in the high-spin Q_t values than the square-root dependence adopted in Ref. [7]. The absolute, and relative, Q_t values at intermediate spins reported here are, however, independent of any such model assumptions and, at least for the cases of the GSB and Band B, independently reveal the rapid increase in Q_t below the paired band crossing. Furthermore, we note that the adopted square-root dependence of the Q_t values in the high-spin unpaired regime provides a considerably better description of the theoretically predicted spin dependence [cf. Fig. 5(b)] than, for example, a linear change in Q_t that would serve to partially smooth the discontinuity between the high- and intermediate-spin results. We therefore retain the assumed square-root dependence of Ref. [7] in the comparison of the high-spin data with the intermediate-spin results presented here.

As illustrated in Fig. 3, the CRHB calculations with pairing remove to a large extent this discrepancy for the GSB band: the CRHB Q_t values are larger than the CRMF ones at low spin and they are close to those of the experimental data. The data points at $I = 8, 10\hbar$ are very well described but the experimental value at $I = 6\hbar$ is underestimated in the CRHB calculations. Because the CRHB calculations are performed as a function of rotational frequency they are not able to describe in detail (as a function of spin) the band-crossing region. They also do not include the configuration mixing and angular momentum projection. These limitations are removed in the generator coordinate method calculations with Skyrme force [GCM(Skyrme)] of Ref. [6] and VAMPIR calculations of Ref. [5]. The GCM(Skyrme) calculations reproduce well the data point at $I = 6\hbar$ but do not reproduce the data point at $I = 8\hbar$ and do not provide any information on whether the drastic drop in Q_t is expected with increasing spin.

The VAMPIR calculations describe the magnitude of the drop of collectivity with increasing spin reasonably well. However, they underestimate the current experimental data by $\approx$0.5 eb but are very close to those of Ref. [13].

The drop of collectivity with increasing spin in the GSB band in spin range $I = 64$–$14\hbar$ is $\sim$0.9 eb. It is clear from Figs. 3 and 4 that the majority of this drop in g band is associated with the paired band crossing that develops at $I \geqslant 12\hbar$ and that is due to simultaneous alignment of the $g_{9/2}$ proton and neutron pairs.

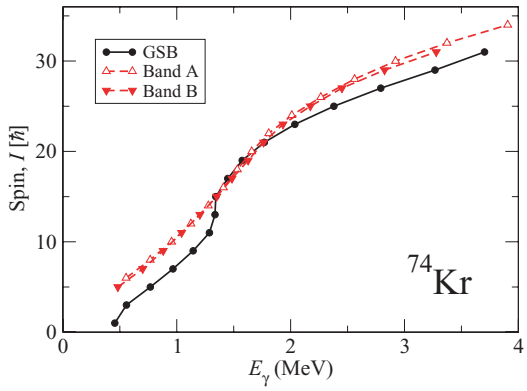

FIG. 4. (Color online) Alignments of ground-state band, band A, and band B in ^{74}Kr as a function of γ-transition energies.

According to the present experiment, the drastic drop of collectivity with increasing spin is seen also in Bands A and B (see Fig. 3). In Band A the collectivity drops by $\sim$0.7 eb when going from $I = 11\hbar$ to $I = 13\hbar$. Such a big change corresponds to a drop by $\sim$20% of the total value of Q_t within one transition. However, it should be noticed that Band A has only one experimental point below $I = 13\hbar$ and therefore it is difficult to obtain a definite conclusions about this drop. In addition, previous measurements of Ref. [13] do not show any drop of collectivity in the spin range of interest. In Band B the collectivity drops by $\sim$1.0 eb when going from $I = 10\hbar$ to $I = 16\hbar$.

The CRHB formalism has not yet been developed for the calculation of two-quasiparticle configurations in even-even nuclei. The quadrupole moment of the negative-parity band was calculated as the expectation value from the wave function at the minimum of the Routhian surface in the TRS approach in Ref. [13]. These calculations did not show any drastic increase of Q_t at low spin (see Fig. 3 in Ref. [13]), which contradicts the experimental data. Here we will try to obtain a general understanding of the low-spin properties of negative-parity bands using an unpaired formalism as a starting point.

The deformation of the nuclear system in a specific configuration is predominantly defined by the shell structure [20]. However, the pairing has some impact on the position of the minima in the potential energy surface. In the calculations without pairing, all single-particle states below (above) the Fermi level are occupied (unoccupied). When the pairing is switched on, the single-particle orbitals in the vicinity of the Fermi level become partially occupied and emptied depending on whether the orbitals are located above or below the Fermi level. For example, in the GSB band the occupation probability of the deformation-driving $N = 4$ proton 1/2[440], 3/2[431], and 5/2[422] states is 0.872, 0.56, and 0.08 in the CRHB calculations at spin 0, whereas in the calculations without pairing only $\pi 1/2[440]$ state is occupied. There are thus two deformation driving $N = 4$ ($g_{9/2}$) protons in the unpaired case compared with approximately three in the paired case.

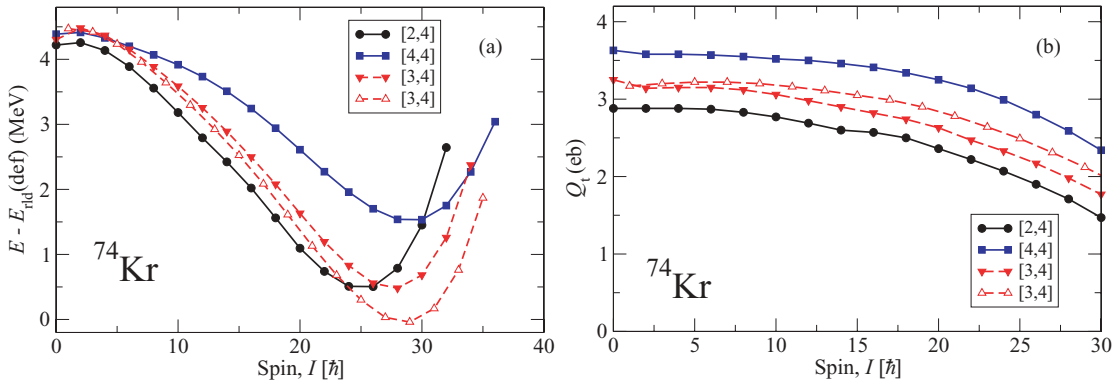

FIG. 5. (Color online) (a) Calculated energies in the CNS formalism according to Ref. [22] shown relative to a rotating liquid drop reference. (b) Calculated Q_t values for the bands shown in panel (a).

The final equilibrium deformation in the presence of pairing as compared with the results of the calculations without pairing depends on (i) whether this redistribution of occupation of single-particle orbitals due to pair scattering leads to an increase or a decrease of the occupation of deformation-driving orbitals and (ii) the deformation dependence of pairing energies. For the GSB band of ^{74}Kr, the presence of pairing leads to an increase of the calculated Q_t value (CRHB value) by $\sim$10% at low spin (with maximum difference at $I \sim 8\hbar$) as compared with the CRMF results without pairing. This result is in agreement with experimental data. The increase is due to partial occupation of the deformation-driving states above the Fermi level in the presence of pairing as stated above. It is interesting to mention that a similar increase (by $\sim$ 5%) in the quadrupole moments due to pairing has previously been reported in the superdeformed bands of the $A \sim 190$ mass region (see Fig. 4 in Ref. [21]).

The paired configuration is a mixture of several unpaired configurations and thus its properties are defined by the properties of the involved unpaired configurations and the weights with which they appear in the structure of the paired configuration. To illustrate this, we consider some important unpaired configurations in ^{74}Kr. Their energies are plotted in Fig. 5. In the unpaired formalism, the GSB band is formed from the [2,4] configuration for all spin values. One notes, however, that the [4,4] configuration comes very close in energy at low-spin values. Therefore, the scattering of proton $g_{9/2}$ pair becomes energetically favorable in the presence of pairing and these two unpaired configurations will have almost the same weights in the structure of the paired configuration of the GSB band. Such a mixture appears consistent with the occupation of the $N = 4$ orbitals in the CRHB calculations specified above. The transition quadrupole moments in the unpaired CNS calculation are plotted in Fig. 5. At low spins, the Q_t value for the [2,4] configuration is around 2.9 eb, whereas the one for the [4,4] configuration is 3.7 eb. Therefore, with equal weights of these two configurations, a Q_t value of approximately 3.3 eb is expected. This corresponds to an increase of 0.4 eb over the Q_t value of the pure [2,4] configuration that is of the same magnitude as the difference between the Q_t values of the CRMF [2,4] configuration and the CRHB GSB configuration at low spin.

The negative-parity Bands A and B are described by the [3,4] configuration at high spin in the unpaired formalism. The Q_t values for these configurations calculated in the CNS formalism are shown in Fig. 5. As would be expected, these values come out roughly as the average of the values for the [2,4] and [4,4] configurations. Other unpaired configurations having negative parity like [5,4], [1,4], [3,2], and [3,6] are calculated much higher in energy. Therefore, one would also expect that with pairing included, these negative-parity Bands A and B will be dominated by the [3,4] configuration with small amplitudes of the configurations having either more or fewer $g_{9/2}$ particles. However, these small amplitudes are not expected to lead to any large corrections of the quadrupole moments. Thus, the pairing correlations are not expected to lead to any large increase of quadrupole moment over the low-spin Q_t values of the unpaired [3,4] configurations. One should also note that Bands A and B are two-proton-quasiparticle configurations. In these configurations, the pairing correlations in the proton subsystem are considerably smaller than in the configuration assigned to the GSB band due to the blocking effect. Thus, the difference in the Q_t values at low spin of the paired configurations and its unpaired high-spin analog ([3,4]) should be smaller than in the case of GSB band.

Our analysis suggests that at low spin, the transition quadrupole moments of the GSB band and the Bands A and B should be similar because the negative-parity bands have predominantly pure [3,4] structure at low spin and the GSB band is expected to have an average of three proton plus four neutron $g_{9/2}$ particles as discussed above. This is also supported by the fact that the Q_t values calculated at low spin for the negative-parity bands in the CRMF formalism are similar to those calculated in the CRHB formalism for the GSB band. Thus, the fact that the experimental Q_t values of the negative-parity bands are larger (especially the high value for the Band A at $I = 11$) than the ones for the GSB band is difficult to understand.

Similar to experiment, going to higher spin values, the unpaired Q_t values for the fixed configurations in Fig. 5 decrease gradually. This can be understood from the gradual alignment corresponding to a tendency for the matter distribution to be concentrated around the equator of the nucleus, i.e., in the plane perpendicular to the rotation axis. This will lead to a

somewhat decreased deformation, cf. Ref. [13], which in turn makes it easier for the angular momenta to align.

The drastic increasing in collectivity at low spin with decreasing spin should also be reflected in the rotational properties, because deformation and rotational properties are correlated. This correlation is clearly seen in the alignment curve of the GSB band (see Fig. 4) where the simultaneous alignments of proton and neutron $g_{9/2}$ pairs lead to a considerable increase of alignment at the band crossing and consequently a large jump in the Q_t value. On the contrary, only a neutron $g_{9/2}$ pair could align in Bands A and B at the paired band crossing, because the alignment of the proton $g_{9/2}$ pair is blocked. The alignment of the neutron $g_{9/2}$ pair is very gradual and in general it should not introduce the sharp increase of Q_t at low spin observed in experiment.

Going beyond the band-crossing region, the alignment in all three bands is similar as seen in Fig. 4. This alignment will then influence the Q_t values for the three bands in a similar way and the fact that the values are somewhat higher in the negative-parity bands is understood from the number of deformation-driving $g_{9/2}$ particles, being $3 + 4 = 7$ in the negative-parity bands but only $2 + 4 = 6$ in the GSB band. The fact that the values appear somewhat larger in Band A than in Band B is explained in the CNS and CRMF formalisms by a tendency for negative γ values in Band A leading to somewhat increased Q_t values.

IV. SUMMARY

Summarizing, the lifetimes of the low-spin states in three bands of ^{74}Kr have been measured using the DSAM method. Together with the previously measured transition quadrupole moments Q_t at high spin [7], this data set provides information about evolution of the Q_t in almost the whole spin range where these bands were observed. Although the calculations without pairing provide good description of the high-spin data, reasonable agreement with experiment at low spin for the ground-state band is obtained in theoretical approaches based on the mean-field concept (CRHB) and the ones [VAMPIR, GMC(Skyrme)] that go beyond mean field. However, the large observed transition probabilities in the negative-parity bands (Band A and Band B) at $I \approx 13\hbar$ remains theoretically unexplained.

ACKNOWLEDGMENTS

This work has been partially supported by the NSERC of Canada, the BMBF of Germany under contract number 06K167, the U.K. Engineering and Physical Sciences Research Council, the Swedish Science Research Council, and the U.S. Department of Energy under contract numbers DE-AC03-76SF00098, DE-FG02-88ER-40406, DE-FG02-07ER41459, and DE-F05-96ER-40983.

[1] E. Bouchez *et al.*, Phys. Rev. Lett. **90**, 082502 (2003).
[2] A. Görgen *et al.*, Eur. Phys. J. A **26**, 153 (2005) (and references therein).
[3] W. Korten, Nucl. Phys. **A752**, 255c (2005).
[4] E. Clement *et al.*, Phys. Rev. C **75**, 054313 (2007).
[5] K. W. S. A. Petrovici and A. Faessler, Nucl. Phys. **A665**, 333 (2000).
[6] M. Bender, P. Bonche, and P.-H. Heenen, Phys. Rev. C **74**, 024312 (2006).
[7] J. J. Valiente-Dobón *et al.*, Phys. Rev. Lett. **95**, 232501 (2005).
[8] B. Cederwall, Nucl. Instrum. Methods A **354**, 591 (1995).
[9] I.-Y. Lee, Nucl. Phys. **A520**, 641c (1990).
[10] D. G. Sarantites, P. F. Hua, M. Devlin, L. G. Sobotka, J. Elson, J. T. Hood, D. R. LaFosse, J. E. Sarantites, and M. R. Maier, Nucl. Instrum. Methods A **381**, 418 (1996).
[11] C. E. Svensson *et al.*, Nucl. Instrum. Methods A **396**, 228 (1997).
[12] J. J. Valiente-Dobón *et al.*, Phys. Rev. C **71**, 034311 (2005).
[13] A. Algora *et al.*, Phys. Rev. C **61**, 031303(R) (2000).
[14] J. C. Wells and N. R. Johnson, ORNL Physics Division Progress Report, No. ORNL-6689, 1991.
[15] J. F. Ziegler and W. K. Chu, At. Data Nucl. Data Tables **13**, 463 (1974).
[16] C. J. Chiara, D. R. LaFosse, D. G. Sarantites, M. Devlin, F. Lerma, and W. Reviol, Nucl. Instrum. Methods A **523**, 374 (2004).
[17] A. V. Afanasjev, D. B. Fossan, G. J. Lane, and I. Ragnarsson, Phys. Rep. **322**, 1 (1999).
[18] A. V. Afanasjev, J. König, and P. Ring, Nucl. Phys. **A608**, 107 (1996).
[19] A. V. Afanasjev and S. Frauendorf, Phys. Rev. C **71**, 064318 (2005).
[20] S. G. Nilsson and I. Ragnarsson, *Shapes and Shells in Nuclear Structure* (Cambridge University Press, New York, 1995).
[21] A. V. Afanasjev, P. Ring, and J. Konig, Nucl. Phys. **A676**, 196 (2000).
[22] B. G. Carlsson and I. Ragnarsson, Phys. Rev. C **74**, 011302(R) (2006).